Research Article | Vol. 30, No. 19 / 12 Sep 2022 / Optics Express 34287
Optics EXPRESS

Phase interrogation of plasmonic tilted fiber Bragg grating biosensors through the Jones formalism

HADRIEN FASSEAUX,[1,3] MÉDÉRIC LOYEZ,[2] KARIMA CHAH,[1] AND CHRISTOPHE CAUCHETEUR[1,*]

[1]Department of Electromagnetism and Telecommunication, University of Mons, 31 Bld Dolez, 7000 Mons, Belgium
[2]Department of Proteomics and Microbiology, University of Mons, 6 Av. Du Champs de Mars, 7000 Mons, Belgium
[3]Hadrien.FASSEAUX@umons.ac.be
[*]christophe.caucheteur@umons.ac.be

Abstract: Gold-coated tilted fiber Bragg gratings (TFBG) are refined plasmonic biosensors, highly sensitive to surrounding refractive index (RI) changes. Their interrogation usually relies on insertion loss measurements for single input polarized light, limiting the set of exploitable features. To overcome this limitation, we trigger the Jones formalism to retrieve the polarization enabling optimized plasmonic excitation for both phase and amplitude measurements. We present an experimental phase shift with a sensitivity as high as 45835°/RIU and further assess this approach to HER2 proteins sensing at 1μg/ml. We compare this angular modality with the one relying on the insertion loss using a quality factor that takes the shift as well as the dispersion into account. This strengthens its relevance in terms of precision for ultra-small RI variations.

1. Introduction

Surface plasmons (SP) belong to the surface wave class propagating along a metal film. As an extension of the plasma theory, an SP is a non-radiative wave associated with an electron density fluctuation excited by light through a prism or grating coupler [1]. The most widely used coupling method relies on the prism coupler in Kretschmann-Raether configuration where light is coupled toward a nanoscale metal-coated surface in contact with the dielectric medium. As a surface wave, the electromagnetic field of the SP decays exponentially in the direction perpendicular to the surface. As a result, SP is sensitive to the dielectric medium characterized by its refractive index (RI). When light is p-polarized, the SP excitation produces a minimum in the reflected intensity and a sharp change in the reflected phase difference between the p and s-polarized light [2–4]. For many years, surface plasmon resonance (SPR) has led to photoelectric enhancements for solar cell improvement [5] or second harmonic generation [6]. Furthermore, the RI sensitivity of SP aroused the interest to include them in ultrasensitive devices such as physical [7,8], chemical and biological sensors [9–12]. To this aim, physical platforms based on optical fibers with various geometries have been investigated [10,13–16] because they are flexible, cost-effective, small-sized and reliable. Among them, gold-coated tilted fiber Bragg gratings (TFBGs) are convenient platforms for biosensing [17]. The grating inside the core of the optical fiber outcouples the forward propagating core mode (HE_{11}) to backward propagating cladding modes [18] resulting in a comb-like shape transmission amplitude spectrum. By coating the fiber with a metal layer (typically gold with a thickness of 50 nm), and immersing the fiber into a dielectric fluid, the transmission spectrum of the p-polarized light displays the characteristic attenuation of SP excitation. Thus, when the refractive index of the surrounding medium (SRI) changes, the transmission spectrum is impacted. This makes

#463140 https://doi.org/10.1364/OE.463140
Journal © 2022 Received 5 May 2022; revised 4 Aug 2022; accepted 19 Aug 2022; published 6 Sep 2022

Optics EXPRESS

gold-coated TFBGs relevant for biodetection owing to SRI changes due to coupling between analytes and receptors grafted on the gold layer. Several demodulation methods can be used to extract the RI changes [19]. One of the latest analyses, which has shown a sensitivity around 560 nm / RIU, consists in tracking the crossing point between the both, top and bottom envelopes of the insertion loss spectrum [20]. Considering that gold-coated TFBGs are transpositions of the Kretschmann-Raether configuration, another feature deserves attention. Indeed, it is well known that phase analysis is another efficient way to improve SPR detection in Kretschmann-Raether configuration [21–23]. However, it is seldom investigated because it often relies on complex optical configuration and interferometric system. In this paper we propose a demodulation method based on phase analysis via Jones matrix manipulation. Introduced by R.C. Jones in 1941 [24], this matrix is a powerful tool to investigate polarization in an optical system. We first measure phase sensitivity of a gold-coated TFBG and after surface functionalization, we apply this method on a detection of human epidermal growth factor receptor-2 (HER2/neu, c-erbB2), an oncogene that is overexpressed and plays an important role in the pathogenesis of human breast cancer [25,26]. Results are confronted with the cross-demodulation analysis, which has already proved its efficiency in previous works using the same and experimental configuration [20].

2. Material and method

2.1. Grating inscription and coating

We use a silica telecommunication-grade optical fiber (Corning SMF-28) and in order to increase the fiber photosensitivity for grating inscription, the SMF-28 is first hydrogen loaded at ~ 200 bar and 60°C for 30 h. Then, using the phase mask technique [27] and a 193 nm excimer laser (Noria from Northlab Photonics), we inscribe a 1 cm long grating with a tilt angle of 8° and a period of 555.41 nm. The hydrogen excess is then removed by a heating process at 100°C for 24 h. Finally, a gold layer with a thickness of 50 nm is coated using a sputter-coater Spuco with 2" magnetron modules with 250 W RF power supply and an inbuilt quartz microbalance with a resolution of 0.1 nm (tectra gmbh, Germany).

2.2. Refractometric calibration

SRI sensitivity of the sensor is determined by immersing the fiber into aqueous LiCl solutions (anhydrous, 99%, from Alfa Aesar) with different RI. Thirty-five solutions have been prepared in order to span RI range at ~ 1550 nm from 1.3161 ± 10^{-4} (pure water) to 1.3229 ± 10^{-4} [20]. These latter have been measured thanks to a portable refractometer (Reichert Analytical instruments, Brix/RI-chek) and then converted to the wavelength of interest using Sellmeier's dispersion relation [28].

2.3. Biofunctionalization process and detection

The specificity of the sensors relies on the grafted bioreceptors used to detect HER2 proteins (116 kDa, Abcam, ab60866). These receptors are thiolated aptamers (5'-TCT AAA AGG ATT CTT CCC AAG GGG ATC CAA TTC AAA CAG C-S-S-3', Glen Research Sterling,VA, USA) reduced according to the same protocol as our previous works [20,29] to allow their direct binding on gold. The fiber is then immersed in this aptamers solution for 1 h to ensure strong binding with the gold layer. A rinsing process with PBS is used to remove unbound receptors. To prevent any undesirable detection, we block the surface with a solution of 5 mM 6-mercapto-1-hexanol in PBS from Sigma Aldrich for 30 min. After a last rinsing with PBS, the biosensor is placed into a 120μl microfluidic chamber (microfluidic ChipShop) where the detection is performed.

Optics EXPRESS

3. Results and discussion

3.1. Sensors transmission and phase spectra

At a given wavelength, the evolution of a totally coherent field propagating through an optical system can be modeled using the Jones formalism. According to the latter, the relationship between an input polarization state, written using the Dirac representation of the Jones vector $|g\rangle \in \mathbb{C}^{2X1}$, and the corresponding output state $|e\rangle$ is

$$|e\rangle = \mathbb{J}|g\rangle, \tag{1}$$

where $\mathbb{J} \in \mathbb{C}^{2x2}$ is the Jones matrix written in a Cartesian coordinate system. Jones matrices of the gold-coated TFBG immersed into aqueous solution are obtained from an optical vector analyzer (OVA, OVA CTE from Luna Technologies Inc.) while the fiber is connected in transmission. To prevent any undesirable polarization effects, the fiber is immobilized and its total length does not exceed 50 cm. In order to use the envelope crossing based demodulation method, we have to extract the insertion loss spectrum of the p-polarized mode. This mode corresponds to a polarized light which oscillates parallel to the tilted plane defined by the grating. Without loss of generality, we can consider that the tilted plane is not necessarily aligned with the axis of the Cartesian coordinate where the Jones matrices are given and we first need to determine the angle between them. To this aim, we know that if we connect the fiber to a linear polarizer that makes an angle θ relative to the x-axis of the coordinate system, the Jones matrix of the whole system (device + polarizer) $\mathbb{J}_{dp}$ becomes

$$\mathbb{J}_{dp} = \mathbb{J}\mathbb{R}\begin{pmatrix} 1 & 0 \\ 0 & 0 \end{pmatrix}\mathbb{R}^{-1}, \tag{2}$$

where $\mathbb{R}$ is the rotation matrix defined by

$$\mathbb{R} = \begin{pmatrix} \cos\theta & -\sin\theta \\ \sin\theta & \cos\theta \end{pmatrix}. \tag{3}$$

Then, we compute the transmitted intensity I corresponding to an input state $|g\rangle$ and given by the Rayleigh quotient

$$I = \frac{\langle g|\mathbb{J}_{dp}^{\dagger}\mathbb{J}_{dp}|g\rangle}{\langle g|g\rangle}, \tag{4}$$

with

$$I \in \{\rho_{min}, \rho_{max}\}, \tag{5}$$

where ρ_{min}, ρ_{max} are respectively the minimum and maximum eigenvalues of the hermitian matrix $\mathbb{J}_{dp}^{\dagger}\mathbb{J}_{dp}$. We finally use the relationship [18]

$$IL = 10\log_{10}\left(\frac{\rho_{min} + \rho_{max}}{2}\right), \tag{6}$$

to get the insertion loss spectra for the whole set of rotation angles θ. It is well known that the insertion loss spectrum of the p-polarized mode of that Au-TFBG displays a characteristic attenuation around 1543 nm when the fiber is immersed in water [20]. Thus, using Eqs. (4) and (6) θ modification yields to the determination of the angle θ_p associated with the p-polarized mode (see Fig. 1(a)). Indeed, since the p-polarized mode insertion loss spectrum displays a characteristic attenuation, θ_p is thus defined by the angle which leads to such spectrum using

Optics EXPRESS

Eq. (6) This leads to the Jones vectors $|p\rangle$ and $|s\rangle$ characterizing the p and s-polarized modes such as, respectively:

$$|p\rangle = \begin{pmatrix} \cos\theta_p \\ \sin\theta_p \end{pmatrix}, \qquad |s\rangle = \begin{pmatrix} \cos(\theta_p \pm \frac{\pi}{2}) \\ \sin(\theta_p \pm \frac{\pi}{2}) \end{pmatrix} = \begin{pmatrix} \cos\theta_s \\ \sin\theta_s \end{pmatrix}. \tag{7}$$

In order to extract the phase introduced by the optical system to the input modes $|p\rangle$ and $|s\rangle$, we compute the inner product between the input states and the output one $|p'\rangle$ and $|s'\rangle$ taking the argument as follows [30]

$$\phi_p = arg(\langle p|p'\rangle) = arg(\langle p|\mathbb{J}|p\rangle), \tag{8}$$

$$\phi_s = arg(\langle s|s'\rangle) = arg(\langle s|\mathbb{J}|s\rangle). \tag{9}$$

Once both relative phases are obtained, we proceed to the difference between the p and s-mode phases. This phase difference $\delta\tilde{\varphi}_{ps}(\lambda) = \phi_s - \phi_p$, shown in Fig. 1(b), is defined with an added constant value $c(\lambda)$ such that

$$\delta\tilde{\varphi}_{ps}(\lambda) = \delta\varphi(\lambda) + c(\lambda). \tag{10}$$

However, its continuity for a given measurement shows that the constant $c(\lambda)$ can be assumed as wavelength independent (*i.e.* $c(\lambda) \equiv c$). Bragg alignment cannot be performed in the phase difference spectra. Thus, in order to remove the constant values, we analyze the differential phase shift between two neighboring peaks at the respective wavelengths λ_k and λ_l. We have

$$\Delta\varphi_i = \delta\varphi(\lambda_l) + c - \delta\varphi(\lambda_k) - c = \delta\varphi(\lambda_l) - \delta\varphi(\lambda_k), \tag{11}$$

where i is an index used to number the pair of peaks chosen. Figure 2(c) shows corresponding representation of the variable $\Delta\varphi_i$ for four pairs of peaks numbered from $i = 1$ to $i = 4$. These pairs were chosen in the most sensitive area of the insertion loss spectrum, as shown in Fig. 2(a) and (b).

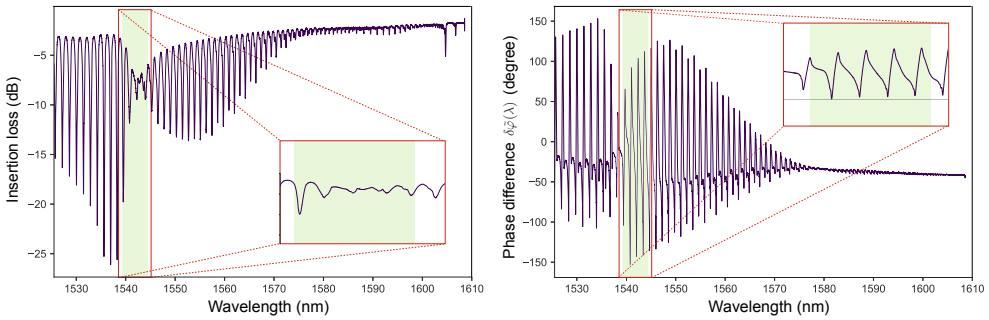

(a) (b)

Fig. 1. (a) Insertion loss of the p-polarized mode. (b) Phase difference spectrum. The insets are a focus on the SPR attenuation wavelength range.

3.2. *Sensitivity of the sensor*

As shown in Fig. 3, when the sensor is immersed in solutions with various RI, the insertion loss spectra as well as the phase difference spectra are modified. The peak pairs of that figure corresponds to $i = 1$, $i = 2$ and $i = 3$ in Fig. 2. To determine the sensitivity of the sensor, two main demodulation methods are usually applied. The most widely used is based on the wavelength evolution of single peaks from the insertion loss spectrum [31]. Using this technique,

Optics EXPRESS

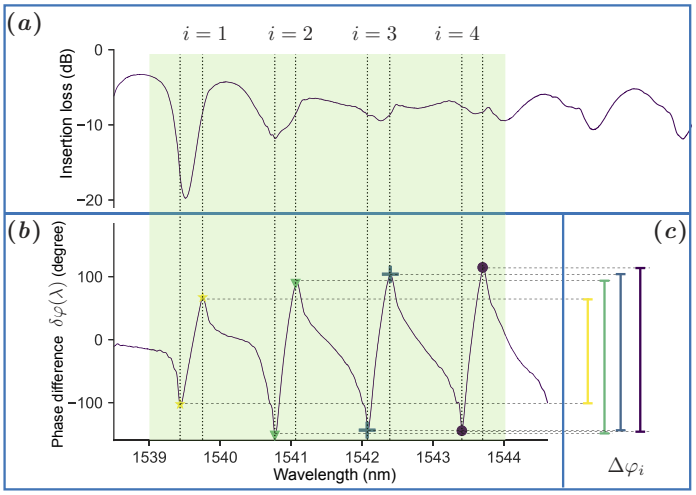

Fig. 2. (a) Insertion loss spectrum spanning the attenuated area (green one). (b) Phase difference in the same range. (c) $\Delta\varphi_i$ visualization for peaks pairs displayed on (b).

we find a sensitivity of 43.56 nm/RIU as shown in Fig. 4(a). This graph shows the relative wavelength shift for 3 different peaks in the insertion loss spectrum (named +1, +2 and +3 in the upper graph of the Fig. 3). The sensitivity is then obtained from the slope of a linear fit. More recently, another technique has shown higher sensitivity than the current peak method. In this method, the insertion loss evolution can be quantified by tracking the wavelength shift of the crossed point between the upper and lower envelope (see Fig. 4(c)). This demodulation [20], leads to a sensitivity of 552.66 nm/RIU as shown in Fig. 4(b). Since the envelope method leads to a sensitivity more than 10 times higher than the peak method, we use it to confront the proposed phase analysis. Unlike the envelope method, the phase difference analysis leads to a sensitivity of $\Delta\varphi_i$ which depends on the pair of peaks chosen. Indeed, Fig. 5 displays the relative $\Delta\varphi_i$ for each of the 4 pairs (named $i = 1$ to $i = 4$ in Fig. 2) showing a slightly asymmetric bell-shaped curve when the RI range is large enough ($i = 1$ and $i = 2$). Because of the asymmetry, the highest sensitivity spans only on one range of RI. Moreover, the RI range with the highest sensitivity of one pair stops where the highest sensitivity range of the next pair starts. Thus, by applying a linear fit through each of these ranges, we extract the phase sensitivity of the gold-coated TFBG, leading to 45835.7°/RIU.

3.3. Biodetection

Considering the aforementioned analysis and because HER2 proteins are diluted in PBS whose RI is measured at 1.3192 ± 10^{-4} at 1542.2 nm, we follow the pair $i = 2$ in Fig. 2. During the first 40 minutes, PBS is injected at a constant flow of 30μŁ/min to ensure reliable probe stability. Then, the HER2 solution progressively replaces PBS in the microfluidic chamber and a first jump followed by a smooth increase is observed. The initial RI jump is related to slight modifications of the medium (bulk RI) while the following progressive shift is related to the binding dynamics between analytes and receptors (surface RI). Because the gold layer is functionalized with anti-HER2 bioreceptors, target proteins remain attached after rinsing. As a result, $\Delta\varphi_2$ does not return to its original level and this difference can be used to assess the RI change due to binding. Figure 6 displays this detection process using the phase difference (Fig. 6(a)) and the insertion loss (Fig. 6(b)). In both cases, the three experimental steps (stabilization, detection, rinsing) are clearly depicted. In order to compare both curves, two dimensionless numbers

Optics EXPRESS

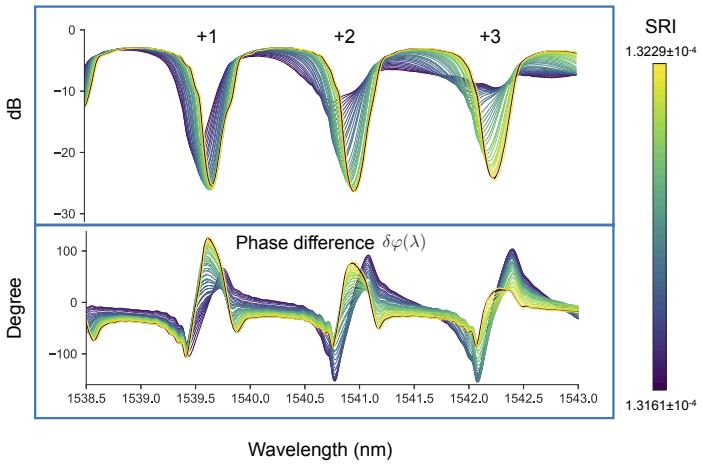

Fig. 3. Evolution of Insertion loss spectra and phase difference spectra with increasing SRI

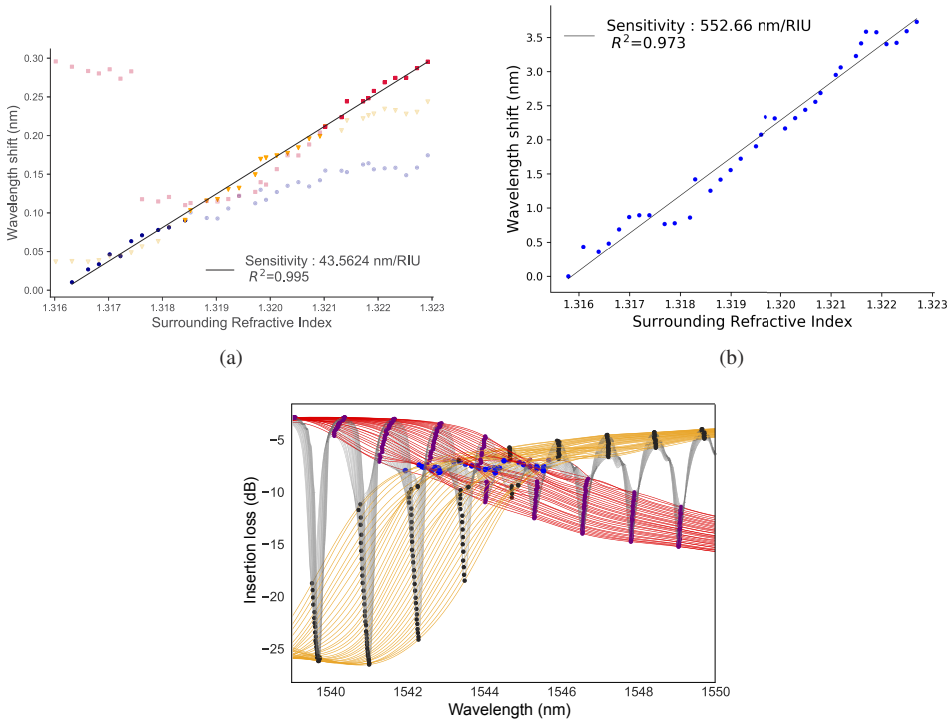

Fig. 4. (a) Peak method applied to peaks numbered +1 to +3 in the upper graph of Fig. 3. Wavelength shift for the 3 peaks are considered and a linear fit is used to extract the sensitivity of the sensor. (b) Spectral envelope demodulation results. The linear fit shows a sensitivity of 552.66 nm/RIU. Data are obtained by following the crossed point of envelopes with increasing RI. (c) Envelope method applied to the insertion loss spectra for sensitivity characterization.

Optics EXPRESS

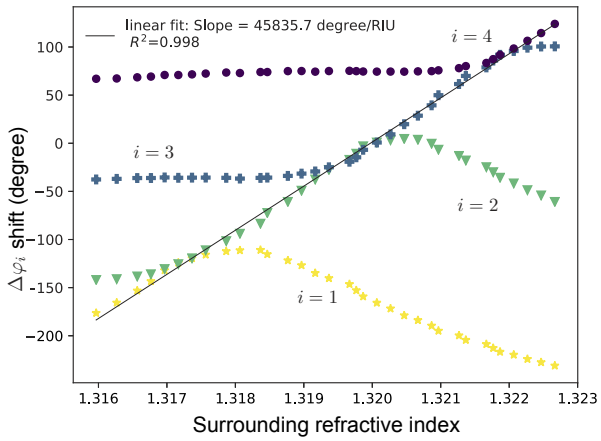

Fig. 5. Relative $\Delta\varphi_i$ shift for a pair of peaks numbered $i = 1$ to $i = 4$.

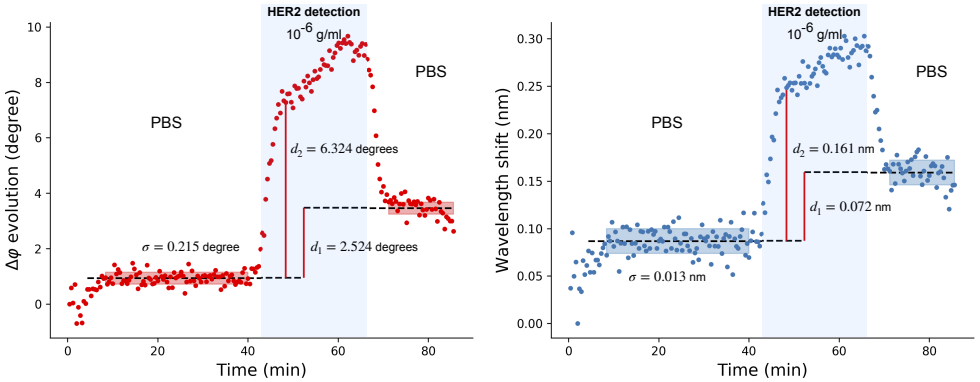

Fig. 6. Detection process. (a) using phase demodulation. (b) using envelope crossing demodulation.

q_1 and q_2 taking the shift as well as the dispersion into account were computed. The shift d_1 is measured using difference between mean values after rinsing and during stabilization. It corresponds to the binding shift while d_2 is used for bulk shift. Then, the standard deviation σ around the mean value during the first step is used to characterize the dispersion. Finally, the dimensionless numbers $q_1 = d_1/\sigma$ and $q_2 = d_2/\sigma$ are computed. By definition of q, the higher value, the better is the curve, either by a reduced dispersion or by higher phase shift. Whether it is for the bulk shift or for the change of RI during the binding process, q parameter is higher with phase demodulation. Considering a sensitivity of 45835.7°/RIU for the phase analysis, one can extract a RI modification due to bulk solution switch of $(13.8 \pm 0.9)\times10^{-5}$ RIU while binding induces $(5.5 \pm 0.9)\times10^{-5}$ RIU. Assuming a Gaussian distribution around the mean value, the error is taken as twice the standard deviation since 95% of the values should be within 2σ of the mean value. Using the insertion loss spectra, RI changes due to the bulk is $(29.1 \pm 2.3)\times10^{-5}$ RIU and RI modification due to binding is $(12.9 \pm 2.3)\times10^{-5}$ RIU. The two shifts using both techniques have the same order (10^{-5} RIU). The difference is assigned to small deviation of the sensitivity extracted on a broad RI variation because of linear fit. The two main features of this advanced phase demodulation can be summarized as

Optics EXPRESS

follows. First, equivalent binding trends were obtained for both transmission parameters (phase difference and amplitude), validating the biodetection process with the established wavelength tracking technique. Second, the phase difference tracking provides noise reduction leading to higher precision. Indeed, the q parameter for binding and bulk are $\{q_1 = 11.7, q_2 = 29.4\}$ and $\{q_1 = 5.5, q_2 = 12.4\}$ for phase demodulation and envelope demodulation respectively. These observations confirm that the phase analysis brings an improved confidence on the detection. This phase demodulation study validated the biodetection by sensorgrams achieved with more generic parameters directly given by the interrogator, without the need for additional polarizer. We pointed out that both methods can be correlated to ensure reliability and extract the RI evolution with high precision.

Results obtained from raw data are summarized in Table 1. The dispersion of the data is reduced thanks to the phase difference analysis improving the fidelity of the detection curves.

Table 1. Data summary (raw data)

	$\Delta\varphi_2$	Spectral envelope intersection
Sensitivity	45835.7°/RIU	552.66 nm/RIU
Standard deviation	0.215°	0.161 nm
RI change due to HER2 solution (10^{-5})	13.8 ± 0.9	29.1 ± 2.3
RI change due to binding (10^{-5})	5.5 ± 0.9	12.9 ± 2.3
q_1 parameter	11.7	5.5
q_2 parameter	29.4	12.4

4. Conclusion

Gold-coated TFBGs are highly sensitive biosensing platforms thanks to the use of fast and easy computed demodulation techniques applied to their insertion loss spectra. To improve the result quality, we have exploited the Jones formalism to extract the phase difference between two orthogonal states of polarization. The phase difference analysis has lead to RI sensitivity as high as 45835.7°/RIU. This demodulation was successfully applied on the biodetection of HER2 proteins and compared with the results achieved through envelopes intersection on insertion loss spectra. We have shown consistent evolution between both methods with a less dispersed signal using the phase difference. We have defined a quality parameter q as the ratio between the monitored shift and twice the standard deviation around the mean while fiber is immersed in the buffer. We have shown a q parameter two times higher for the phase demodulation method compared to the standard amplitude analysis, confirming the precision improvement linked to the phase read-out. Furthermore, this new demodulation process does not rely on interpolations which reduces the potential computing deviation of the real values, leading to promising prospects for the detection of ultra-small surface refractive index variations, such as those provoked by biological or chemical reactions.

Funding. Fonds De La Recherche Scientifique - FNRS.

Acknowledgments. This work was financially supported by the Fonds de la Recherche Scientifique - F.R.S.- FNRS under Senior Research Associate Grant of Christophe Caucheteur and the postdoctoral research grant of Médéric Loyez (C.R.), the PDR Mosaic and EOS n° O001518F (EOS-convention 30467715).

Disclosures. The authors declare no conflict of interest.

Data Availability. Data underlying the results presented in this paper are not publicly available at this time but may be obtained from the authors upon reasonable request.

Optics EXPRESS

References

1. H. Raether, "Surface plasmons on smooth surfaces," in *Surface plasmons on smooth and rough surfaces and on gratings*, (Springer, 1988), pp. 4–39.
2. R. Kaňok, D. Ciprian, and P. Hlubina, "Surface plasmon resonance-based sensing utilizing spatial phase modulation in an imaging interferometer," Sensors **20**(6), 1616 (2020).
3. P. Hlubina, M. Lunackova, and D. Ciprian, "Phase sensitive measurement of the wavelength dependence of the complex permittivity of a thin gold film using surface plasmon resonance," Opt. Mater. Express **9**(3), 992–1001 (2019).
4. H. R. Gwon and S. H. Lee, "Spectral and angular responses of surface plasmon resonance based on the Kretschmann prism configuration," Mater. Trans. **51**(6), 1150–1155 (2010).
5. J. Jacak and W. Jacak, "Plasmon-induced enhancement of efficiency of solar cells modified by metallic nano-particles: material dependence," J. Appl. Phys. **124**(7), 073107 (2018).
6. M. A. Vincenti, D. de Ceglia, C. D. Angelis, and M. Scalora, "Surface-plasmon excitation of second-harmonic light: emission and absorption," J. Opt. Soc. Am. B **34**(3), 633 (2017).
7. J. K. Sahota, N. Gupta, and D. Dhawan, "Fiber Bragg grating sensors for monitoring of physical parameters: a comprehensive review," Opt. Eng. **59**(06), 1 (2020).
8. O. V. Butov, A. P. Bazakutsa, Y. K. Chamorovskiy, A. N. Fedorov, and I. A. Shevtsov, "All-fiber highly sensitive Bragg grating bend sensor," Sensors **19**(19), 4228 (2019).
9. J. Homola, "Surface plasmon resonance sensors for detection of chemical and biological species," Chem. Rev. **108**(2), 462–493 (2008).
10. M. Loyez, M. C. DeRosa, C. Caucheteur, and R. Wattiez, "Overview and emerging trends in optical fiber aptasensing," Biosens. Bioelectron. **196**, 113694 (2022).
11. Y. Y. Shevchenko and J. Albert, "Plasmon resonances in gold-coated tilted fiber Bragg gratings," Opt. Lett. **32**(3), 211–213 (2007).
12. M. Loyez, M. Wells, S. Hambÿe, F. Hubinon, B. Blankert, R. Wattiez, and C. Caucheteur, "PfHRP2 detection using plasmonic optrodes: performance analysis," Malar. J. **20**(1), 332 (2021).
13. A. Ortega-Gomez, M. Loyez, M. Lobry, K. Chah, J. Zubia, J. Villatoro, and C. Caucheteur, "Plasmonic sensors based on tilted Bragg gratings in multicore optical fibers," Opt. Express **29**(12), 18469 (2021).
14. T. Guo, H.-Y. Tam, P. A. Krug, and J. Albert, "Reflective tilted fiber Bragg grating refractometer based on strong cladding to core recoupling," Opt. Express **17**(7), 5736 (2009).
15. D. Tosi, "Review and analysis of peak tracking techniques for fiber Bragg grating sensors," Sensors **17**(10), 2368 (2017).
16. F. Chiavaioli, F. Baldini, S. Tombelli, C. Trono, and A. Giannetti, "Biosensing with optical fiber gratings," Nanophotonics **6**(4), 663–679 (2017).
17. C. Caucheteur, J. Villatoro, F. Liu, M. Loyez, T. Guo, and J. Albert, "Mode-division and spatial-division optical fiber sensors," Adv. Opt. Photonics **14**(1), 1–86 (2022).
18. A. Bialiayeu, A. Ianoul, and J. Albert, "Polarization-resolved sensing with tilted fiber Bragg gratings: Theory and limits of detection," J. Opt. **17**(8), 085601 (2015).
19. M. Vidal, M. S. Soares, M. Loyez, F. M. Costa, C. Caucheteur, C. Marques, S. O. Pereira, and C. Leit ao, "Relevance of the spectral analysis method of tilted fiber Bragg grating-based biosensors: a case-study for heart failure monitoring," Sensors **22**(6), 2141 (2022).
20. M. Lobry, H. Fasseaux, M. Loyez, K. Chah, E. Goormaghtigh, R. Wattiez, F. Chiavaioli, and C. Caucheteur, "Plasmonic fiber grating biosensors demodulated through spectral envelopes intersection," J. Lightwave Technol. **39**(22), 7288–7295 (2021).
21. R. Miyan, X. Wang, J. Zhou, Y. Zeng, J. Qu, H.-P. Ho, K. Zhou, B. Z. Gao, J. Chen, and Y. Shao, "Phase interrogation surface plasmon resonance hyperspectral imaging sensor for multi-channel high-throughput detection," Opt. Express **29**(20), 31418–31425 (2021).
22. D. Sotnikov, A. Zherdev, and B. Dzantiev, "Detection of intermolecular interactions based on surface plasmon resonance registration," Biochemistry **80**, 1820–1832 (2015).
23. Y. Huang, H. P. Ho, S. K. Kong, and A. V. Kabashin, "Phase-sensitive surface plasmon resonance biosensors: methodology, instrumentation and applications," Ann. Phys. **524**(11), 637–662 (2012).
24. R. C. Jones, "A new calculus for the treatment of optical systems. description and discussion of the calculus," J. Opt. Soc. Am. **31**(7), 488–493 (1941).
25. D. J. Slamon, G. M. Clark, S. G. Wong, W. J. Levin, A. Ullrich, and W. L. McGuire, "Human breast cancer: correlation of relapse and survival with amplification of the HER-2/neu oncogene," Science **235**(4785), 177–182 (1987).
26. C. Gutierrez and R. Schiff, "HER2: biology, detection, and clinical implications," Arch. Pathol. Lab. Med. **135**(1), 55–62 (2011).
27. R. Kashyap, "Chapter 3 - fabrication of Bragg gratings," in *Fiber Bragg Gratings*, R. Kashyap, ed. (Academic Press, Boston, 2010), pp. 53–118, second edition ed.
28. M. Daimon and A. Masumura, "Measurement of the refractive index of distilled water from the near-infrared region to the ultraviolet region," Appl. Opt. **46**(18), 3811–3820 (2007).

Optics EXPRESS

29. M. Loyez, M. Lobry, E. M. Hassan, M. C. DeRosa, C. Caucheteur, and R. Wattiez, "HER2 breast cancer biomarker detection using a sandwich optical fiber assay," Talanta **221**, 121452 (2021).
30. J. C. Gutiérrez-Vega, "Optical phase of inhomogeneous jones matrices: retardance and ortho-transmission states," Opt. Lett. **45**(7), 1639–1642 (2020).
31. M. Loyez, M. Lobry, R. Wattiez, and C. Caucheteur, "Optical fiber gratings immunoassays," Sensors **19**(11), 2595 (2019).